

Research Article

Studies on the Improvement of Efficient Selection and Focus Field Coil Configurations

Julia Mrongowius · Christian Kaethner* · Thorsten M. Buzug*

Institute of Medical Engineering, Universität zu Lübeck, Lübeck, Germany

*Corresponding author, email: {kaethner,buzug}@imt.uni-luebeck.de

Received 27 November 2015; Accepted 27 May 2016; Published online 03 June 2016

© 2016 Mrongowius; licensee Infinite Science Publishing GmbH

This is an Open Access article distributed under the terms of the Creative Commons Attribution License (<http://creativecommons.org/licenses/by/4.0>), which permits unrestricted use, distribution, and reproduction in any medium, provided the original work is properly cited.

Abstract

Magnetic Particle Imaging is an imaging modality that detects the distribution of magnetic tracer material. By use of oscillating magnetic fields, a tracer signal can be generated in a defined field of view (FOV). In order to specify the region, where a signal can be detected, a selection field can be used that features a field free point (FFP). The FFP is steered around in the FOV to achieve a spatial encoding. Due to technical and medical limitations, the FOV that can be covered by such an FFP is very limited. However, an enlargement of the FOV is possible by use of focus fields. Instead of using separate electromagnetic coils to generate the selection field and the focus field, a combined coil assembly that generates both magnetic fields can be used. Such a coil configuration, combining the features of a classical Maxwell coil setup and a single-sided coil arrangement, allows for a very power efficient way to generate these magnetic fields. In this work, different studies are carried out to improve such a combined coil assembly with respect to the electrical power loss.

1. Introduction

Magnetic Particle Imaging (MPI) is an imaging method that is capable of detecting the distribution of superparamagnetic iron oxide particles due to their nonlinear magnetization behavior [1]. The signal generation can be achieved by oscillating magnetic fields, known as drive fields, that are generated by electromagnetic coils. In order to realize a spatial encoding, an additional magnetic gradient field, known as the selection field, is superimposed to the drive fields. The selection field features a low magnetic field region, e.g. a field free point (FFP), where the highest particle signal can be achieved. A movement of such an FFP allows for a signal encoding of defined areas. Due to technical and medical limitations [2], the size of this area is strongly limited. A possibility to overcome this limitation is by use of additional focus fields [1, 3]. Whereas the drive fields enable a fast FFP movement, the focus fields feature a rather slow movement of the FFP. As

for example described in [4], it is possible to generate the selection field and the focus fields by combined selection and focus field (SeFo) coils.

A power efficient concept for a combined SeFo coil configuration was presented for a 1D scenario in [5]. The concept combines a classical Maxwell coil configuration and a single-sided coil setup [6] in one coil assembly. An extension of the 1D principles to multiple dimensions was described in [7]. Both works focused primarily on an efficient transition from preclinical developments to human sized MPI systems [4, 8]. Such an upscaling of an MPI scanning device and the involved electromagnetic coils leads to an immensely increased electrical power loss for the generation of a selection and focus field.

In this work, different simulation studies are performed that focus on possibilities to improve an efficient SeFo field coil arrangement. In this context, a curved rectangular coil featuring a radial curvature is introduced to allow for a further reduction of the electrical power loss.

II. Material and Methods

In this section, the used material and applied methods are presented. First, a reference setup is defined as a basis for the subsequent improvement procedure regarding the electrical power loss. Afterwards, the current optimization used for the simulation studies is described. Due to the fact that the choice of the coil geometry can have an immense impact on the power optimization, the selection of the used coil geometry is described. The section concludes with a description of the simulation studies.

II.I. Reference Setup

The coil configuration that serves as a reference for the simulation studies is described in detail in [7]. The setup consists of an outer and an inner ring of coils. Each ring of coils features four coil pairs of two interleaved coils. An example visualization of the coil arrangement is illustrated in Fig. 1.

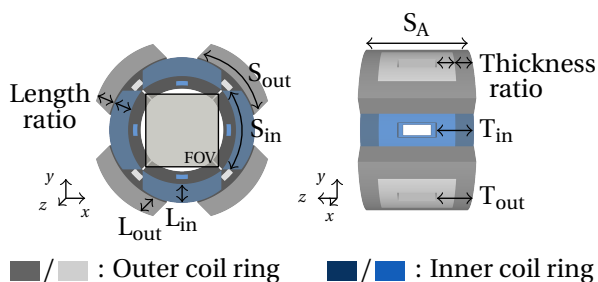


Figure 1: Illustration of the reference coil configuration and the coil dimensions relevant for the simulation studies.

The respective values for the coil dimensions are for the side lengths $S_A = 40$ cm as well as $S_{in} = 31.42$ cm and $S_{out} = 31.42$ cm. The length of the coils is given by $L_{in} = 7.05$ cm and $L_{out} = 7.05$ cm, and the thickness is $T_{in} = 13.1$ cm and $T_{out} = 13.1$ cm. Thus, the length ratio and the thickness ratio are 1:1. For all described parameters, the index “in” refers to the inner ring of coils close to the FOV, while “out” describes the outer ring of coils. The curvature C of the coils is chosen with respect to the enclosed cylindrical bore that has a diameter of 40 cm. These parameters result in a total coil volume of 0.068 m^3 . The copper fill factor of each coil of this configuration is assumed to be 0.8.

II.II. Current Optimization

In order to ensure a minimal electrical power consumption, the simulated electrical currents for each coil configuration are optimized as proposed in [5, 7]. The magnetic field simulations are carried out under the assumption of the Bio-Savart law and, in order to simulate the volume coils, discretized current densities are used.

II.III. Selection of the Coil Geometry

A cylindrical patient access is assumed for the coil configurations in this work. It has been shown in [9] that for such a patient access curved rectangular coils are an excellent choice, because of featuring a low electrical power loss as well as a high field homogeneity. Based on these findings, only curved rectangular coils are used for the coil arrangements in this work (see Fig. 2). In terms of the curvature, a radially curved rectangular coil geometry (rad) is proposed in addition to conventionally curved rectangular coils (con). The geometry adaption causes a different distribution of the discretized current densities and aims for a further reduction of the power loss by fully enclosing the FOV.



Figure 2: Illustration of a) a conventionally curved rectangular coil (con) and b) a radially curved rectangular coil (rad) as well as c) a visual comparison of both geometries.

II.IV. Simulation Studies

The performed simulation studies are separated into two parts: i) an improvement assuming a constant coil volume, ii) an improvement based on a variable coil volume. The calculations for the current optimization and therefore the electrical power loss are carried out in a FOV discretized into 101×101 positions. The size of the considered FOV is $28 \times 28\text{ cm}^2$, i.e. 70 % of the actual bore size of 40 cm. The gradient strength is given by $1.5\text{ Tm}^{-1}\mu_0^{-1}$ in y direction and $0.75\text{ Tm}^{-1}\mu_0^{-1}$ in x and z direction. The coil configurations are iteratively improved and after each iteration the parameters are revalidated with the already improved measures of the setup.

Improvement based on a Constant Coil Volume

The main objective in the first part of the improvement study is to reduce the electrical power loss while maintaining the total coil volume. The reason of a constant total coil volume, i.e. a constant amount of copper, during the improvement is to ensure a fair comparison between the developed coil arrangements. In addition to the total coil volume, the diameter of the cylindrical bore size is kept constant. Thus, the improvement of each coil in the setup is limited to small changes in the side length (S_{in} , S_{out}), the length (L_{in} , L_{out}), and the curvature type (C) (see Fig. 1).

Improvement based on a Variable Coil Volume

In the second part of the improvement study, the coil volume is neglected. Thus, it is studied how certain parameter changes, ratios, and combinations independent from the coil volume influence the electrical power loss. The coils are changed with respect to the overall length ($L_{in} + L_{out}$), the length ratio (L_{in}/L_{out}), side lengths (S_{in} , S_{out}), the overall thickness ($T_{in} + T_{out}$), the thickness ratio (T_{in}/T_{out}) and the curvature type (C) (see Fig. 1).

III. Results

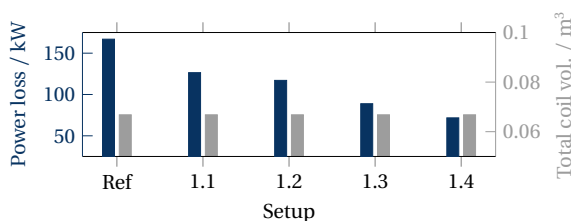
In this section, the results of the improvement studies are given. For all improvements, a range of parameter combinations is iteratively changed and cross validated with previously improved parameters. In the following, the results are limited to selected setups. Due to simplification with respect to the improved parameters, only the parameters for the outer coils of each coil ring are described. Note that in this work the focus is mainly on the reduction of the electrical power loss. The field quality in terms of, e.g. the field homogeneity, is neglected.

Improvement based on a Constant Coil Volume

In Tab. 1, selected setup parameters for the improvement based on a constant total coil volume and the respective electrical power losses are given. In addition to that, the maximal current density of all coils of the respective setup is given by J_{max} . Due to a possible increase of the coil volume during the procedure, each step will feature a way to adapt the coil volume to the reference value of 0.068 m^3 .

Table 1: Overview of selected values during the improvement based on a constant coil volume. The values in the first four rows are given in cm, while the values in the last row are given in A/mm^2 . The graph below shows the maximum electrical power loss and the total coil volume for the considered setups.

	Ref	1.1	1.2	1.3	1.4
S_{in}	31.42	31.42	31.42	31.00	31.00
S_{out}	31.42	42.49	41.38	31.66	40.61
L_{in}	7.05	7.05	6.35	6.22	5.70
L_{out}	7.05	5.64	6.35	6.22	5.70
C	con	con	con	rad	rad
J_{max}	14.28	15.81	16.73	8.93	9.20



In the first step, from the reference setup to setup 1.1, the gaps on the outer ring of coils are closed. Thus, the power loss can be reduced by 25 % to 126.43 kW. The reduction of the coil volume to 0.068 m^3 is realized by decreasing L_{out} . A further power reduction to 117.08 kW is achieved in setup 1.2 by changing the coil dimensions. Here, the volume reduction is done by decreasing the length of both, L_{out} and L_{in} , while the length ratio is 1:1. In setup 1.3, a power loss reduction by another 25 % from 117.08 kW to 88.85 kW without closing the outer coil gaps is possible by the use of radially curved coils (rad). The last setup considered here, i.e. setup 1.4, is based on fully enclosing the FOV with radially curved coils (rad) and improving the coil parameters. Thus, the power loss can be reduced to 71.73 kW. This means that while the total coil volume remains constant, a reduction of the power loss by 57 % is possible. As done before, the reduction of the coil volume to the reference volume is achieved by decreasing L_{in} and L_{out} , whereas the ratio remains 1:1. An alternative approach of decreasing $T_{in} + T_{out}$ results in less power efficient coil configurations. A visualization of setup 1.2 and setup 1.4 can be seen in Fig. 3. Considering J_{max} in each setup, it can be observed that the current density can be decreased by the use of the radially curved coil (rad). The amount of the maximal current density is considerable lower after the substitution of the coil geometry in setup 1.3.

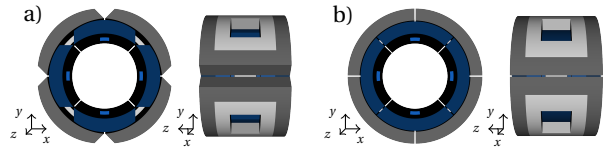


Figure 3: Visualization of a) setup 1.2 and b) setup 1.4. For both setups a frontal and a side view are shown.

Improvement based on a Variable Coil Volume

In this part, the results based on a variable total coil volume are presented. The improved parameters of selected setups and the corresponding electrical power losses are given in Tab. 2. Again, J_{max} names the maximal current density of the individual coils in each setup. For simplification the thickness in Tab. 2 is given as the total thickness over the inner and outer coils (see also Fig. 1).

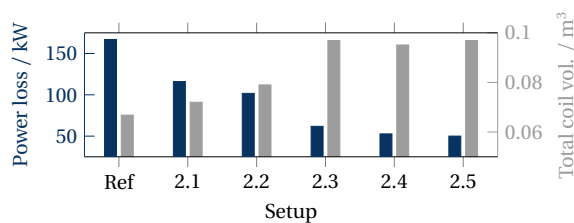
A first power reduction to 116.04 kW (see setup 2.1) can be achieved by an improvement of $L_{in} + L_{out}$, L_{in}/L_{out} , and T_{in}/T_{out} . The parameter $L_{in} + L_{out}$ is increased to 15.2 cm, L_{in}/L_{out} is 1:4, and T_{in}/T_{out} is about 1:1.2. In setup 2.2, the power loss can be further decreased to 101.75 kW by increasing S_{out} . Another high reduction of the power loss is possible by the use of radially curved coils (rad) in setup 2.3. While the total coil volume is increased by almost 23 %, the power loss can simultane-

ously be reduced to 61.86 kW. In the step from setup 2.3 to setup 2.4, the parameters $T_{in} + T_{out}$ and T_{in}/T_{out} are improved, which results in an overall thickness of 15 cm for the inner coils and 17 cm for the outer coils. The ratio T_{in}/T_{out} for the inner ring of coils is about 1:6.5 and about 1:4.5 for the outer ring of coils.

A subsequent improvement of $L_{in} + L_{out}$ and L_{in}/L_{out} results for setup 2.4 in a power loss of 50.05 kW. The value of $L_{in} + L_{out}$ is increased to 15.6 cm, while the L_{out} remains constant and only L_{in} is increased by 0.4 cm, so that L_{in}/L_{out} is slightly changed to 1:3.5. Thus, in comparison to the reference setup, the power loss can be reduced by 70 %. Setup 2.2 and setup 2.5 are shown in Fig. 4. Regarding the current density, one can depict that

Table 2: Overview of selected values during the improvement based on a variable coil volume. The values in the first four rows are given in cm, while the values in the last row are given in A/mm². The graph below shows the maximum electrical power loss and the total coil volume for the considered setups.

	Ref	2.1	2.2	2.3	2.4	2.5
S_{out}	31.42	31.42	36.91	36.91	36.91	37.45
L_{in}	7.05	3.04	3.04	3.04	3.04	3.44
L_{out}	7.05	12.16	12.16	12.16	12.16	12.16
S_A	40	40	40	40	35.75	35.75
T_{in}	13.1	13.1	13.1	13.1	15	15
T_{out}	13.1	13.1	13.1	13.1	17	17
C	con	con	con	rad	rad	rad
J_{max}	14.28	30.82	31.88	11.74	22.99	22.31



again the use of the radially curved coil (rad) as well as a high amount of copper decreases J_{max} . Since in the setups 2.3, 2.4, and 2.5 only the distribution of the volume of the coils is changed, one can see that this apparently has a high impact on the current densities as well.

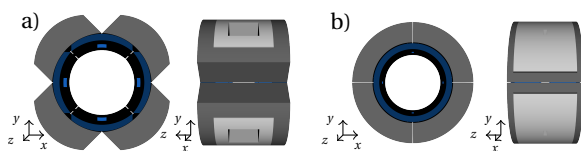


Figure 4: Visualization of a) setup 2.2 and b) setup 2.5. For both setups a frontal and a side view are shown.

IV. Conclusion

In this work, two different simulation studies have been carried out to improve an efficient SeFo coil assembly. The first study concentrated on an improvement based on a constant coil volume, whereas the second study neglected the coil volume. As a part of the improvement studies, a radially curved rectangular coil (rad) has been introduced in addition to the conventionally curved one (con). The main observation in this work is that it is possible to reduce the electrical power loss with and without a volume constraint on the simulation. The substitution of the coil geometry by the radially curved coil and, with that, the fully enclosed FOV shows to have a great influence on the reduction of the power loss in both studies.

The reduction of the electrical power loss is an important enhancement for the realization of an efficient SeFo generator. However, in a realization, several technical obstacles have to be taken into account.

For example, regarding the current densities of the individual coils, it can be concluded, that this value has to be further reduced in order to realize an efficient SeFo generator. In order to take account of that and a further reduction of the electrical power loss, the here presented scanner setups could be tested with superconductive or soft iron coils in further simulation studies. In addition, the parameter S_A affects the power loss also in a significant way and should be considered in a separate simulation study more precisely.

In a realization of the scanner setup, heat development is a quite presumable issue. Since the improvements in this study go along with a closing of the gaps in between the coils, it might be more complicated to cool the coil system. Though, it would be interesting for future work to look at the heat development and a potential way of cooling. For further considerations or towards a possible realization of the presented improved scanner setup, also the field quality has to be taken into account.

References

- [1] B. Gleich and J. Weizenecker. Tomographic imaging using the nonlinear response of magnetic particles. *Nature*, 435(7046):1214–1217, 2005. doi:[10.1038/nature03808](https://doi.org/10.1038/nature03808).
- [2] E. U. Saritas, P. W. Goodwill, G. Z. Zhang, and S. M. Conolly. Magnetostimulation limits in magnetic particle imaging. *IEEE Trans. Med. Imag.*, 32(9):1600–1610, 2013. doi:[10.1109/TMI.2013.2260764](https://doi.org/10.1109/TMI.2013.2260764).
- [3] I. Schmale, J. Rahmer, B. Gleich, J. Kanzenbach, J. D. Schmidt, C. Bontus, O. Woywode, and J. Borgert. First phantom and in vivo mpi images with an extended field of view. In *SPIE Medical Imaging*, 2011. doi:[10.1117/12.877339](https://doi.org/10.1117/12.877339).
- [4] C. Bontus, B. Gleich, B. David, O. Mende, and J. Borgert. Concept of a generator for the selection and focus field of a clinical mpi scanner. *IEEE Trans. Magn.*, 51(2):6502004, 2015. doi:[10.1109/TMAG.2014.2326003](https://doi.org/10.1109/TMAG.2014.2326003).
- [5] T. Knopp and T. M. Buzug. *Magnetic Particle Imaging: An Introduction to Imaging Principles and Scanner Instrumentation*. Springer, Berlin/Heidelberg, 2012. doi:[10.1007/978-3-642-04199-0](https://doi.org/10.1007/978-3-642-04199-0).

- [6] T. F. Sattel, T. Knopp, S. Biederer, B. Gleich, J. Weizenecker, J. Borgert, and T. M. Buzug. Single-sided device for magnetic particle imaging. *J. Phys. D: Appl. Phys.*, 42(1):1–5, 2009. doi:[10.1088/0022-3727/42/2/022001](https://doi.org/10.1088/0022-3727/42/2/022001).
- [7] C. Kaethner, M. Ahlborg, T. Knopp, T. F. Sattel, and T. M. Buzug. Efficient gradient field generation providing a multi-dimensional arbitrary shifted field-free point for magnetic particle imaging. *J. Appl. Phys.*, 115(4):044910–1–044910–5, 2014. doi:[10.1063/1.4863177](https://doi.org/10.1063/1.4863177).
- [8] J. Borgert, J. D. Schmidt, I. Schmale, C. Bontus, B. Gleich, B. David, J. Weizenecker, J. Jockram, C. Lauruschkat, O. Mende, M. Heinrich, A. Halkola, J. Bergmann, O. Woywode, and J. Rahmer. Perspectives on clinical magnetic particle imaging. *Biomed. Tech. / Biomed. Eng.*, 58(6):551–556, 2013. doi:[10.1515/bmt-2012-0064](https://doi.org/10.1515/bmt-2012-0064).
- [9] M. Erbe, T. F. Sattel, and T. M. Buzug. Improved field free line magnetic particle imaging using saddle coils. *Biomed. Tech. / Biomed. Eng.*, 58(6):577–582, 2013. doi:[10.1515/bmt-2013-0030](https://doi.org/10.1515/bmt-2013-0030).